

FILAMENTS IN GALACTIC WINDS DRIVEN BY YOUNG STELLAR CLUSTERS

A. RODRÍGUEZ-GONZÁLEZ¹, A. ESQUIVEL¹, P. F. VELÁZQUEZ¹, A. C. RAGA¹, V. MELO

Draft version August 21, 2021

ABSTRACT

The starburst galaxy M82 shows a system of H α -emitting filaments which extend to each side of the galactic disk. We model these filaments as the result of the interaction between the winds from a distribution of Super Stellar Clusters (SSCs). We first derive the condition necessary for producing a radiative interaction between the cluster winds (a condition which is met by the SSC distribution of M82). We then compute 3D simulations for SSC wind distributions which satisfy the condition for a radiative interaction, and also for distributions which do not satisfy this condition. We find that the highly radiative models, that result from the interaction of high metallicity cluster winds, produce a structure of H α emitting filaments, which qualitatively agrees with the observations of the M82, while the non-radiative SSC wind interaction models do not produce filamentary structures. Therefore, our criterion for radiative interactions (which depends on the mass loss rate and the terminal velocity of the SSC winds, and the mean separation between SSCs) can be used to predict whether or not an observed galaxy should have associated H α emitting filaments.

Subject headings: Hydrodynamics – shock waves – star: winds, outflows – galaxies: star cluster – galaxies: starburst – galaxies: individual: (M82, NGC253)

1. INTRODUCTION

Supergalactic winds are a very important mechanism in the evolution of the Universe. Lynds & Sandage (1963) found a large outflow in M82 and gave the first definition of a starburst. They proposed that material was ejected from the nuclear regions as the consequence of a SN explosion. Different analytical models have been put forward to explain the so-called supergalactic winds (SGWs), see, e. g., the work of Chevalier & Clegg (1985), Tomisaka & Ikeuchi (1988), Heckman et al (1990), Leitherer & Heckman (1995), Strickland & Stevens (2000), Cantó et al (2000), Tenorio-Tagle et al. (2003), and Cooper et al. (2008). In the nearest starbursts, they have shown that the supergalactic winds (SGW) form through the collective effects of many individual stellar cluster winds, which are in turn formed by the collective effect of many individual stellar winds.

The best-studied starburst galaxy is M82. It has an extended, biconical filamentary structure in the optical (Shopbell & Bland-Hawthorn 1998; Ohyama et al. 2002). This optical emission is embedded in a pool of soft X-ray emission, detected with the Chandra X-Ray Observatory (Griffiths et al. 2000) as well as with XMM-Newton (Stevens et al. 2003). This X-ray emission extends several kpc away from the nuclear region, into the IGM.

With the Hubble Space Telescope (HST), it has been possible to isolate the building blocks of some starbursts: Super Stellar Clusters (SSCs). These objects are very massive and dense stellar clusters, with masses in excess of $10^4 M_{\odot}$ enclosed in radii of 3–10 pc. They are young, and typically contain from ~ 100 up to $\sim 10^4$ OB stars. In M82, the SSCs H α luminosities are in the range of $(0.01-23) \times 10^{38}$ erg s⁻¹ (Melo et al 2005). These authors catalogued 197 SSCs in M82 with masses in the

$10^4 < M/M_{\odot} < 10^6$ range. This exceptional density of massive clusters (620 kpc^2) produces a suitable scenario for a study of the interaction between cluster winds.

The differences in the populations of SSCs of several starburst galaxies can help us to understand which properties are more important for producing filaments. For instance NGC253, which does not show a clear filamentary structure (Rice 1993), has a significantly lower SSC mass loss rate than M82. However, other authors claim that the lack of filamentary structure in this galactic wind is simply a result of not having deep enough H α observations of this object (Hoopers et al. 1995). In NGC253 Melo (2005) catalogued a total of 48 SSCs with an average distance between them of 31 pc, in contrast with the mean separation between SSCs of 12 pc found in M82. In M82, a rich structure of filaments, extending out from the galactic plane, is present. There are many other examples such as NGC1569 (Anders et al. 2004; Westmoquette, Smith & Gallagher III 2008) and M83 (Harris et al. 2001), that have high density of SSCs with similar masses to the ones of M82.

Tenorio-Tagle et al. (2003) showed that the interaction of stellar winds from a collection of energetic, neighbouring SSCs could form a filamentary structure similar to the one observed in M82. These authors propose the formation of such filaments by means of supernovae explosions that would expel a huge amount of heavy elements into the Interstellar Medium (ISM), thus enhancing the radiative cooling of the outflows.

In their model, Tenorio-Tagle et al. (2003) explained the SGW structure as a consequence of the interaction of winds from very close SSCs, in which stationary oblique shocks are responsible for shaping the material into dense and cold, kiloparsec-sized filaments. More recently, Cooper et al. (2008) presented a numerical study of a starburst-driven galactic wind. Their setup consisted of a series of neutral dense clouds placed in the galaxy disk. The dense clouds are swept up by the main shock

Electronic address: ary, esquivel, pablo, raga@nucleares.unam.mx, vmelo@iac.es

¹Instituto de Ciencias Nucleares, Universidad Nacional Autónoma de México, Ap. 70-543, 04510 D.F., México

TABLE 1
COOLING DISTANCE AS A FUNCTION OF SHOCK
VELOCITY

v_s [km s ⁻¹]	$\log_{10}(d_{c,1}$ [pc])		
	Z_\odot	$5Z_\odot$	$10Z_\odot$
100	-1.468	-2.010	-2.283
200	-1.194	-1.960	-2.259
300	-0.657	-1.439	-1.796
400	0.595	-0.091	-0.399
500	0.957	0.269	-0.037
600	1.176	0.516	0.209
700	1.449	0.763	0.455
800	1.601	0.913	0.605
900	1.727	1.038	0.714
1000	1.893	1.208	0.900
1100	2.108	1.438	1.123

wave, leaving behind a filamentary structure.

In the present paper, we discuss models for the formation of filamentary structures as the result of the interaction between winds from a system of many clusters with a disk-like spatial distribution. In these models we consider only the flow resulting from the wind interactions, and do not include the effect of the stratified ISM present in the region of the galactic disk.

The paper is organized as follows. In §2, we study which combinations of parameters (mass loss rate \dot{M}_w , cluster wind velocity v_w , and separation between nearby star clusters D) yield a highly radiative SGW flow. In §3 we describe a series of 3D simulations of the interaction of cluster winds in this highly radiative regime. We present predictions of the emission in the optical and X-ray wavelength ranges, and compare them with observations of galactic winds (i.e. M82, NGC253, etc.) in §4. Finally, in §5 we present our conclusions.

2. THE FORMATION OF FILAMENTARY STRUCTURES

2.1. General considerations

The collective effect of the individual stellar winds inside an SSC result in a cluster wind. Outside the outer radius of the cluster (i. e., for radii $r > r_c$, where r_c is the cluster radius), the cluster wind has an approximately constant velocity, and a density that falls $\propto r^{-2}$ (where r is the distance to the cluster centre, see, e. g., Rodríguez-González et al. 2007).

Cold filaments in SGWs can be formed by the interaction of such SSC winds, provided that the cooling is efficient. Since the gas density of the cluster wind falls with distance, this is likely to happen only when the clusters are very close each other. The terminal velocity of the SSC winds and their mass loss rate are also important for determining whether or not we have efficient cooling.

2.2. Radiative losses in a cluster wind

Let us consider a galaxy with a central stellar cluster density n (number of clusters per unit volume). For the sake of simplicity, we consider stellar clusters with identical, isotropic winds, mass loss rate \dot{M}_w , and a terminal wind velocity v_w . The typical separation between stellar clusters is $D \approx n^{-1/3}$.

Therefore, two-wind shock interactions between nearby clusters pair will occur at a typical distance $\sim D/2$ from each of the stellar clusters, so that the pre-shock densities

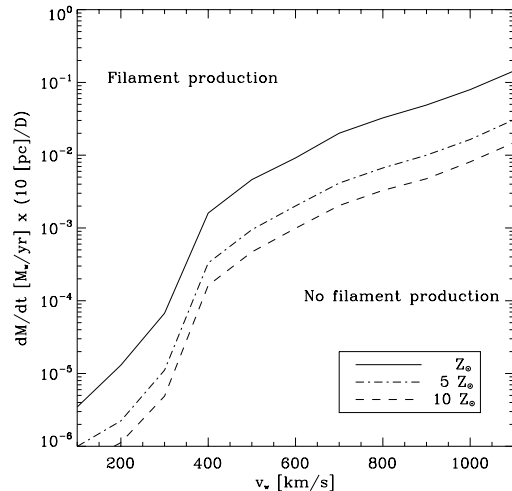


FIG. 1.— This diagram shows $\dot{M}_w \times (10 \text{ pc}/D)$ as a function of v_w (where D is the separation between clusters, \dot{M}_w is the mass loss rate, and v_w the cluster wind velocity) for a “cooling parameter” $\kappa = d_{cool}/D = 1$. Three curves are shown, corresponding to models with 1, 5, and 10 times solar metallicities. The region above the curves represents the parameter space in which the two-wind interactions of cluster winds are radiative.

would have values of

$$n_{pre} = \frac{\dot{M}_w}{1.3m_H\pi D^2v_w}, \quad (1)$$

where m_H is the Hydrogen mass, and we have assumed a 90% H and 10% He particle abundance.

The shock interactions between nearby clusters will be radiative if the cooling distance d_{cool} satisfies the condition

$$\kappa \equiv \frac{d_{cool}}{D} < 1. \quad (2)$$

In order to estimate the cooling distance, we proceed as follows. Consider the structure that will be formed by the leading shock of a star cluster wind with velocity $\approx v_w$ (i. e. the cluster wind velocity) with a preshock density given by equation (1). For a cooling function in the low density regime, the cooling distance scales as the inverse of the pre-shock density, yielding:

$$d_{cool}(n_{pre}, v_s) = \left[\frac{d_{c,1}(v_s)}{n_{pre}} \right], \quad (3)$$

where $v_s (= v_w)$ is the shock velocity, and $d_{c,1}(v_s)$ is the cooling distance (to 10^4 K) behind a shock with $n_{pre} = 1 \text{ cm}^{-3}$. We have calculated the function $d_{c,1}(v_s)$ by integrating the equations for a 1D, stationary shock (see, e. g., Shull & McKee 1979) using the coronal equilibrium cooling functions for 1, 5 and 10 times solar metallicities of Raymond, Cox & Smith (1976). The resulting values of the cooling distance $d_{c,1}(v_s)$ (to 10^4 K, for a $n_{pre} = 1 \text{ cm}^{-3}$ preshock density) are given in Table 1.

Setting $\kappa = 1$ in equation (2) and also using equation (3), one obtains

$$\frac{\dot{M}}{D} = 1.3m_H\pi v_w d_{c,1}(v_w), \quad (4)$$

which gives the relation between \dot{M} , D and v_w for SSCs that are just entering the highly radiative regime. In

Figure 1, we plot the $\frac{\dot{M}}{D}$ ratio as a function of v_w and for SSCs with $\kappa = 1$ (see equation 4) for the three metallicities which we have considered (see above and Table 1). The curves that would be obtained for $\kappa < 1$ always lie above the $\kappa = 1$ curve corresponding to the same metallicity. Figure 1 shows that in a substantial part of the parameter space which would be expected for galaxies with low or intermediate mass young stellar clusters, cooling parameters $\kappa < 1$ are produced. A galactic wind in this “highly radiative regime” will have dense, cool structures resulting from the radiative shocks in the interactions between nearby stellar clusters. In the following section, we present numerical simulations of flows in this regime.

3. NUMERICAL SIMULATION

We have computed 3D numerical simulations with the full, radiative gasdynamic equations. The simulations solve a multiple stellar wind interaction problem with the 3D, adaptive grid “yguazú-a” code, which is described in detail by Raga et al. (2000, 2002). The first four simulations were performed on a five-level binary adaptive grid with a maximum resolution of 0.488 pc (corresponding to $512 \times 512 \times 1024$ grid points at the maximum grid resolution), in a computational domain of $250 \times 250 \times 500$ pc. We have also computed a fifth simulation also on a five-level adaptive grid, but with a maximum resolution of 0.976 pc, corresponding to $1024 \times 1024 \times 2048$ grid points (at the maximum grid resolution) in a domain of $1 \times 1 \times 2$ kpc (see Table 2).

In order to study the formation of filaments in the radiative regime we ran 6 models. We have assumed that the computational domain was filled initially with a homogeneous, stationary ambient medium with temperature $T_{env} = 1000$ K and density $n_{env} = 0.1 \text{ cm}^{-3}$. This environment clearly does not include the ISM of the disk of a starburst galaxy, for which densities of $\sim 1000 \text{ cm}^{-3}$ might be more appropriate. We choose this low density so that the ISM in the region in between the cluster is rapidly flushed away by the cluster winds, and a stationary wind interaction structure is reached as rapidly as possible. If we introduced a higher ISM density (within the galactic plane), there would be a transient regime (lasting longer for higher ISM densities) before the cluster winds break out of the galactic plane and travel into the intergalactic medium. The density which we have chosen is closer to a possible density for the inter galactic medium into which the cluster winds will be expanding once they leave the galaxy.

We model the SSCs as spherical wind sources, centered at the positions as described below. For models M1-M4 (see Table 2), the wind sources have a radius of $R_c = 2.92$ pc (corresponding to 6 pixels at the maximum resolution of the adaptive grid, which is always present at the wind sources), for models M2b and M3b their radii is $R_c = 5.84$ pc (also corresponding to 6 pixels at the highest resolution grid).

Within these spheres, we impose (at every timestep) a wind with a temperature of $T_c = 10^7$ K, an outwardly directed velocity $v_c = 1000 \text{ km s}^{-1}$, and a density that follows an r^{-2} law (where r is the radial coordinate measured outwards from the position of each wind source), scaled so as to obtain the correct the mass loss rate.

The positions of the wind sources are obtained by sampling a uniform random distribution. However, in prac-

TABLE 2
MODEL PARAMETERS

Model	Number of SSCs	Z [Z_\odot]	D^\dagger [pc]	\dot{M}_{SC} [$M_\odot \text{ yr}^{-1}$]
M1	100	1	9.27	2×10^{-2}
M1a	100	1	9.27	2×10^{-1}
M2 [‡]	100	5	9.27	2×10^{-2}
M3 [‡]	100	10	9.27	2×10^{-2}
M4	15	10	21.88	4×10^{-3}
M4a	15	10	21.88	4×10^{-2}

[†]The value quoted here is the mean distance between neighbouring clusters (nearest neighbors) as measured from the positions that result from sampling a uniform random distribution.

[‡]We have also run models M2b and M3b with the same parameters as M2 and M3, but with 1/2 of the spatial resolution and 4 times the spatial extent as M2 and M3.

tice, we have to modify the obtained cluster distributions to avoid the overlap of sources. The stellar cluster sources are placed in a cylindrical structure, meant to model the central region of a galactic disk.

3.1. The starburst regions

In order to reproduce the properties of M82 and of NGC253, we use the average properties reported by Melo et al. (2005) and Melo (2005). For M82, the mean stellar cluster mass (\bar{M}_{SC}) is of $1.7 \times 10^5 M_\odot$, and the mean separation between neighbouring clusters ($\bar{\Delta}$) is of 12 pc. For NGC253, $\bar{M}_{SC} = 6.2 \times 10^4 M_\odot$ and $\bar{\Delta} = 31$ pc. We should note that the clusters of Melo et al. (2005) were detected at optical wavelengths. As there is a high level of obscuration in the nuclear regions of M82 as well as NGC253, the real number of clusters will be larger, and the mean separation between clusters will be smaller than the values quoted above.

We estimate the mass loss rate \dot{M}_{SC} using the starburst 99 models (Heckman & Leitherer 1995, Leitherer et al. 1999²) with the appropriate cluster masses and a Salpeter initial mass function (IMF) including stars between 1 and $100 M_\odot$. The resulting mass loss rate (through winds and supernovae) is reasonably constant after ~ 4 Myr of the onset of the starburst, with some enhancement when input by SNe overcomes the input from winds. This enhancement occurs at around $t \simeq 10$ Myr, and lasts for about 10 Myr, then the mass loss rate returns to a value similar to the pre-supernovae phase for another ~ 20 Myr. Finally, the mass loss rate drops dramatically once the last star of $\sim 8 M_\odot$ explodes as a supernova leaving only intermediate and low-mass star winds (at this point the star cluster would no longer be classified as SSC).

For models M1-M4 we used a constant mass loss rate with a value consistent with the average mechanical luminosity of the SSCs. However, given the assumptions we have made (of having a system of identical clusters with average properties) a larger mass loss rate could be possible, especially if the SSCs are in the SN phase. Such a large mass loss rate could have a significant effect in the production of filaments. For this reason we have run two additional models, M1a and M4a, with extreme values of \dot{M}_{SC} , which correspond to upper limits (within the uncertainties), at the peak of the mass loss rate during the

² <http://www.stsci.edu/science/starburst99/>

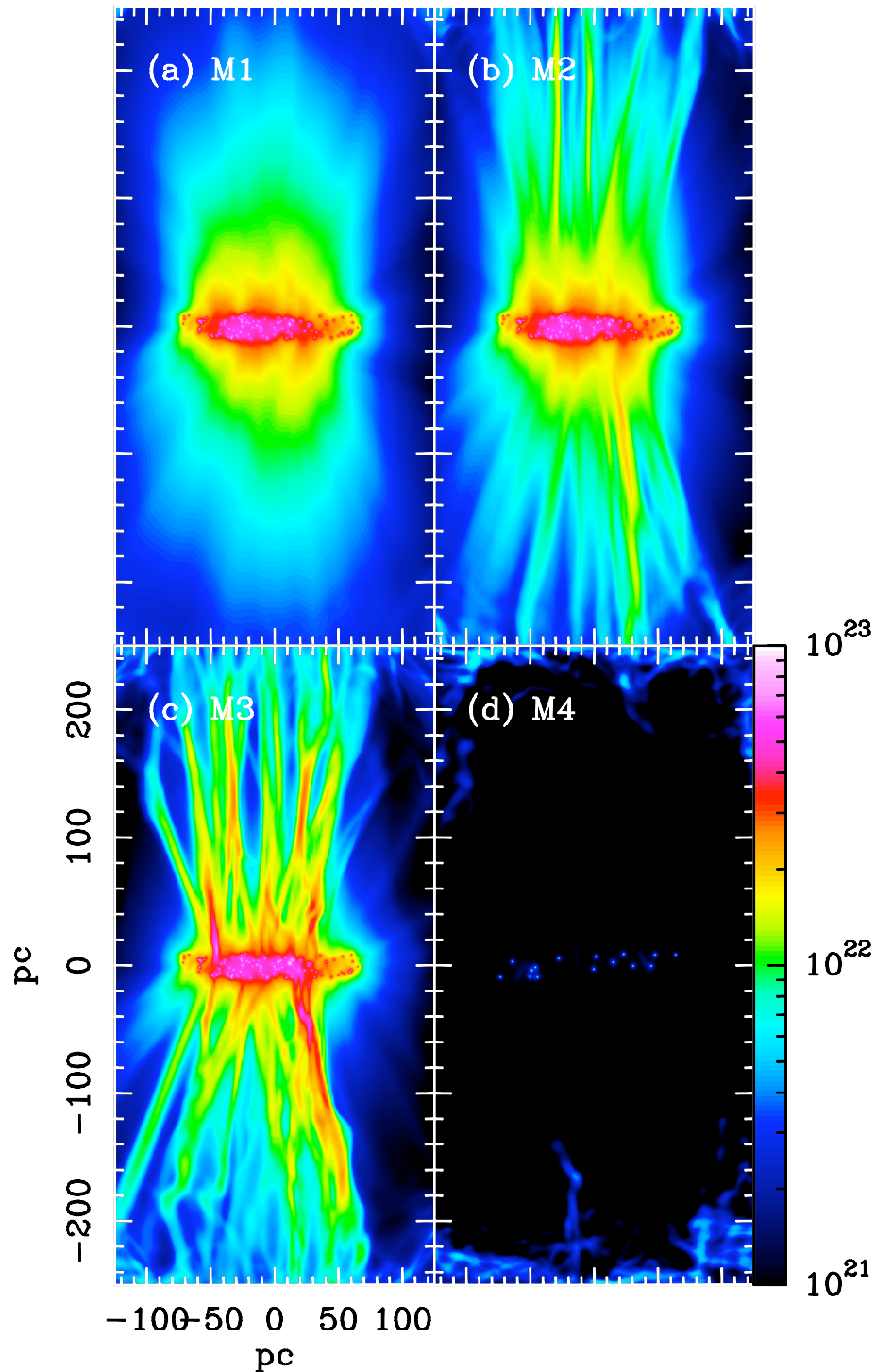


FIG. 2.— Column density maps of models M1-M4. The bar at the bottom right gives the logarithmic gray-scale (color-scale in the online version) in cm^{-2} . The images were obtained by integrating density along lines of sight parallel to the x -axis. The distributions correspond to time-integrations of $(2.5, 2.5, 2.5, 5) \times 10^5$ yr (for models M1-M4, respectively).

SN phase. Aside of the increased mass loss rate, these two models are identical to M1 and M4, respectively (see Table 2).

3.2. The models

We computed four numerical simulations of SGWs driven by stellar clusters, with different metallicities, mass input rates, and number of clusters. All of the models were computed with identical stellar clusters with a cluster wind velocity $v_w = 1000 \text{ km s}^{-1}$, placed in a

cylinder with a radius of 100 pc and a height of 20 pc. This cylinder represents the central part of the starburst in a galaxy as M82, with dimensions approaching those of an individual starburst clump (O’Connell et al. 1995, Westmoquette et al. 2007). In reality the starburst of M82 has spatial extent of ~ 500 pc (see O’Connell & Mangano 1978). Numerical simulations with the full spatial extent for the cluster distribution would be much more demanding computationally. From SB99, using the mean cluster mass for M82 (Melo 2005), we estimate a

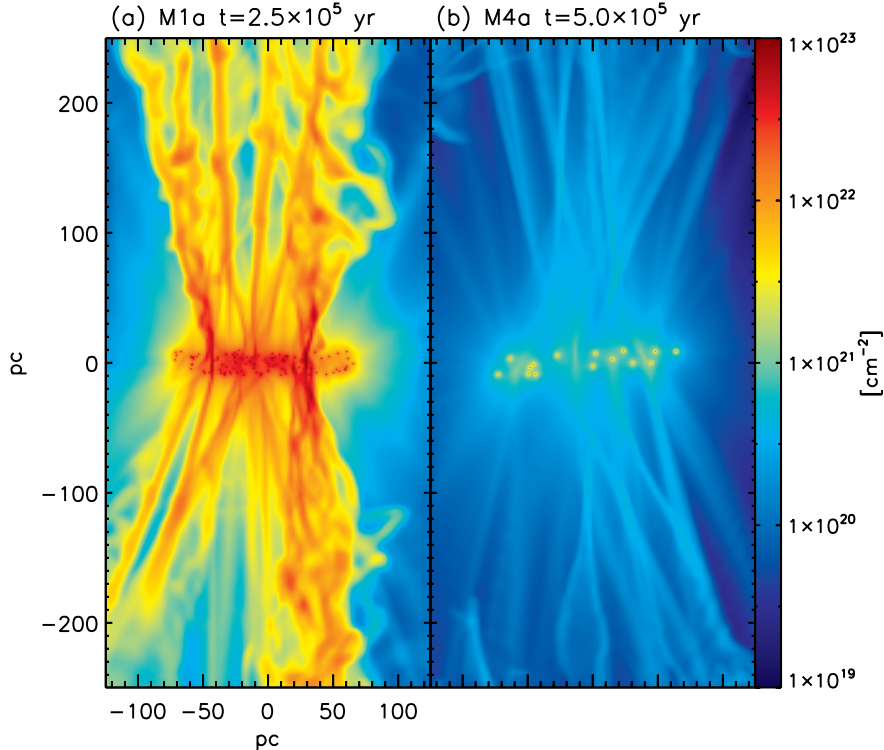


FIG. 3.— Column density maps for the models with mass loss rate in the SN phase (M1a and M4a). The bar at the right gives the logarithmic gray-scale (color-scale in the online version) in cm^{-2} . The images were obtained by integrating the density along lines of sight parallel to the x -axis. The corresponding integration times are of $(2.5, 5) \times 10^5$ yr (for models M1a and M4a, respectively).

mechanical luminosity of 6×10^{39} erg s^{-1} per SSC. Using $\dot{E}_{SC} = \dot{M}_{SC} v_w^2 / 2$ relation, this luminosity translates into a cluster mass loss rate of $\sim 2 \times 10^{-2} M_{\odot} \text{yr}^{-1}$. This cluster mass loss rate has been used for computing models M1, M2, and M3. These three models have different metallicities: $Z = 1, 5$ and $10Z_{\odot}$ (for M1, M2 and M3 respectively).

These metallicities have been chosen as representative values of the metallicities of winds from starbursts during the first 20 Myr time-evolution. Using the metal yields of Meynet & Maeder (2002), Tenorio-Tagle et al. (2005) have shown that the metallicity of the combined stellar winds remains at a value of $\sim 0.5 Z_{\odot}$ up to a $t = 3$ Myr evolutionary time, rapidly grows to $\sim 15 Z_{\odot}$ at $t \approx 7$ Myr, and then gradually decreases to $\sim 3 Z_{\odot}$ at $t \approx 20$ Myr.

Similarly, for NGC253 we obtain a mechanical luminosity of 1.9×10^{39} erg s^{-1} , which corresponds to a cluster mass loss rate $\sim 4 \times 10^{-3} M_{\odot} \text{yr}^{-1}$. This cluster mass loss rate was used for computing model M4.

For models M1-M3, we have placed 100 clusters within the cylindrical volume described in the beginning of this subsection, which results in a mean separation between clusters $D = 9.3$ pc, which is similar to the mean separation $\bar{\Delta} = 12$ pc between the clusters of M82 (see §3.1). Model M4 has a $Z = 10Z_{\odot}$ metallicity, and has 15 clusters within the cylindrical volume, resulting in a mean separation between clusters of $D = 21.9$ pc, which is similar to the mean separation $\bar{\Delta} = 31$ pc between the clusters of NGC253 (see §3.1). The parameters of models M1-M4 are summarized in Table 2.

With these parameters, models M2 and M3 lie above the $\kappa = 1$ curves (for the appropriate metallicities), so

that they are clearly in the highly radiative regime (see Figure 1). Model M1 and M4 lie below the $\kappa = 1$ curves, so that they are not in this regime. Therefore, we would expect to form dense filaments only in models M2 and M3. We evolve models M1, M2, and M3 up to an integration time of $t = 2.5 \times 10^5$ yr, and M4 up to $t = 5 \times 10^5$ yr. In Figure 2, we show the column densities obtained by integrating the number density along the x -axis of the domain, for the flow stratifications obtained at the end of the time-integrations. From this Figure, it is clear that models M2 and M3 produce a structure of $\sim 10 \rightarrow 20$ filaments both above and below the plane of the galactic disk (within which are distributed the SSCs). Models M1 and M4 do not produce filamentary structures.

The bipolar distribution of the filaments is a direct result of the flattened cylindrical distribution of the SSCs (see Figure 2). We have also done simulations in which the cylindrical distribution has a height equal to the diameter (not included in the present paper), and they show filamentary structures with an almost isotropic distribution. The same result is of course also found for a spherically symmetric cluster distribution.

In Figure 3, we present the column density obtained in the models with extreme mass loss rates (M1a and M4a, see Table 2) at $t = 2.5$ and 5×10^5 yr, respectively. Due to the increase of \dot{M} , the cooling distances become an order of magnitude shorter (see the density scaling in equation 3), thus the adimensional parameter κ for M1a and M4a is comparable to that of M3 ($\kappa < 1$). Therefore, as expected, Figure 3 shows filamentary structure, even when it is absent for the same configuration at a lower mass loss.

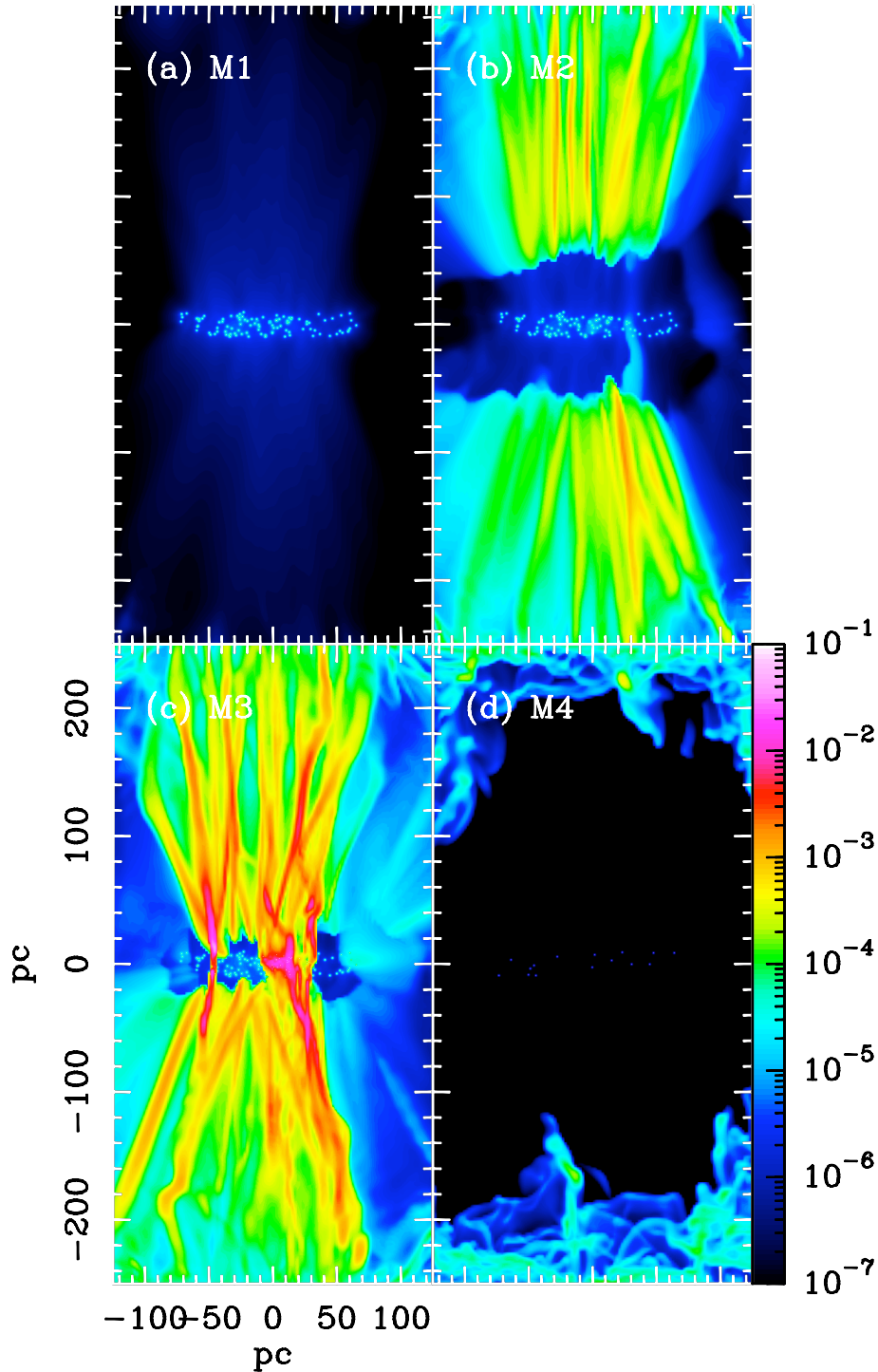


FIG. 4.— $H\alpha$ maps obtained for models M1-M4. The bar at the bottom right, gives the logarithmic gray-scale (color-scale in the online version) in $\text{erg s}^{-1} \text{cm}^{-2} \text{sterad}^{-1}$. The images were obtained by integrating the emission coefficient along lines of sight parallel to the x -axis. The distributions correspond to time-integrations of $(2.5, 2.5, 2.5, 5) \times 10^5$ yr (for models M1-M4, respectively).

4. THE GALACTIC WIND EMISSION

4.1. The $H\alpha$ emission

In Figure 4, we show the $H\alpha$ maps computed by integrating the $H\alpha$ emission coefficient along the x -axis. The emission coefficient is computed with the interpolation formula given by Aller (1987) for the temperature dependence of the recombination cascade.

In model M3, we see a structure of $H\alpha$ filaments which extend out from the galactic plane. In model M2 (which

has lower radiative losses due to its lower metallicity), the $H\alpha$ filaments appear only at a distance of $\sim \pm 50$ pc from the galactic plane. Models M1 and M4 do not produce $H\alpha$ -emitting filaments. The $H\alpha$ filaments in M82 (Ohyama et al. 2002) appear to extend down to the galactic plane, though this effect could partially be due to the fact that the plane of M82 is at an angle of $\sim 10^\circ$ with respect to the line of sight. We would therefore conclude that the $Z = 10Z_\odot$ metallicity model M3 appears to be more appropriate for reproducing the $H\alpha$ filaments

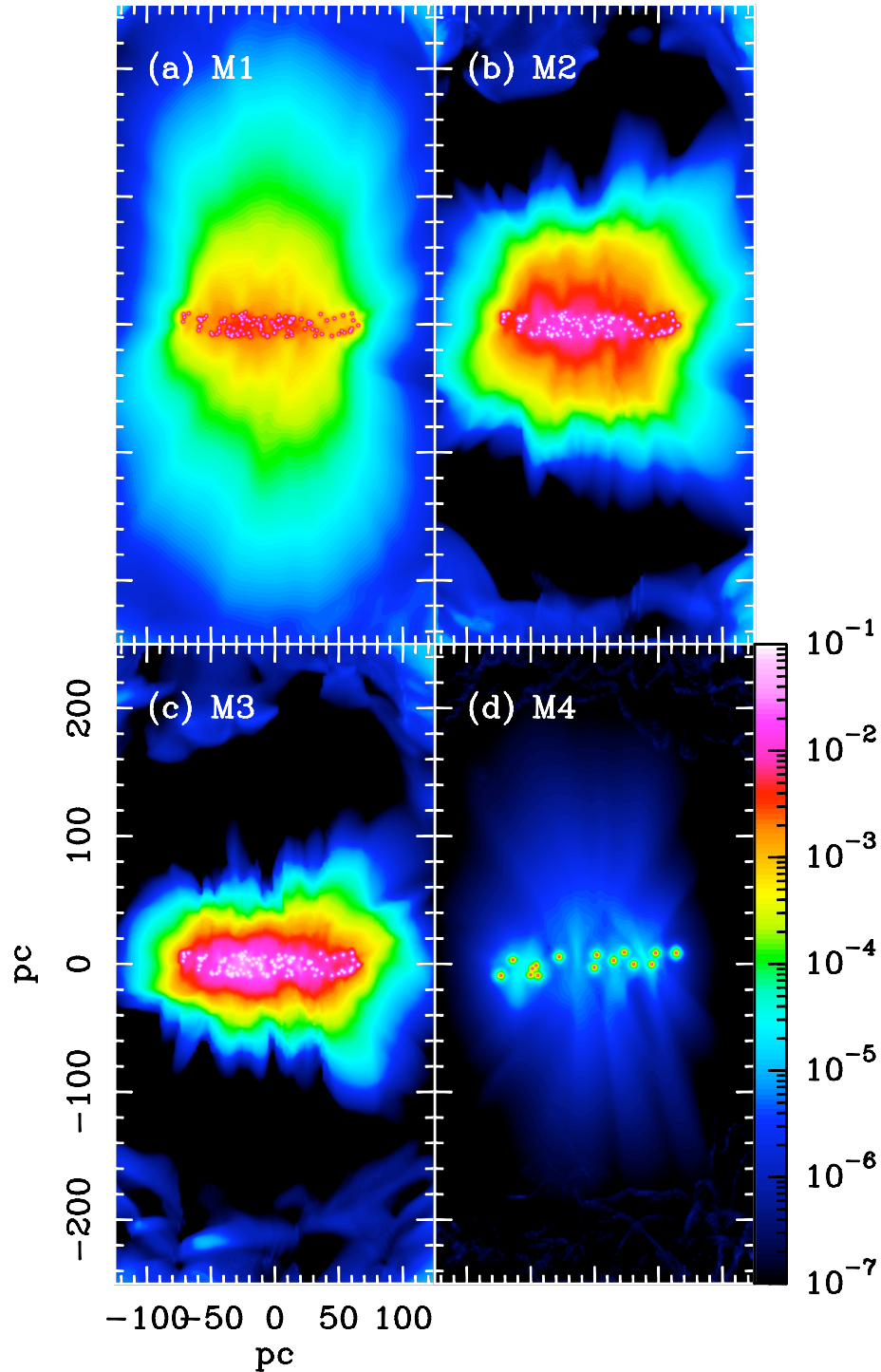


FIG. 5.— X-ray maps for models M1-M4. The bar at the bottom right, gives the logarithmic gray-scale (color-scale in the online version) in $\text{erg s}^{-1} \text{cm}^{-2} \text{sterad}^{-1}$. The images were obtained by integrating the X-ray emission coefficient along lines of sight (parallel to x -axis), in the energy band of 0.3 to 2 keV. The distributions correspond to time-integrations of $(2.5, 2.5, 2.5, 5) \times 10^5$ yr (for models M1-M4, respectively).

of M82.

4.2. The X-Ray emission

We have taken the density and temperature stratifications from the SGW flow configurations, and used them to calculate the X-ray emission. We have done this by computing the emission coefficient in the 0.3 \rightarrow 2 keV

photon energy range using the CHIANTI³ atomic data base and software (see Dere et al. 1997, Landi et al. 2006). For this calculation, it is assumed that the ionization state of the gas corresponds to coronal ionization

³ The CHIANTI database and associated IDL procedures, now distributed as version 5.1, are freely available at: <http://www.solar.nrl.navy.mil/chianti.html>, <http://www.arcetri.astro.it/science/chianti/chianti.html>, and <http://www.damtp.cam.ac.uk/user/astro/chianti/chianti.html>

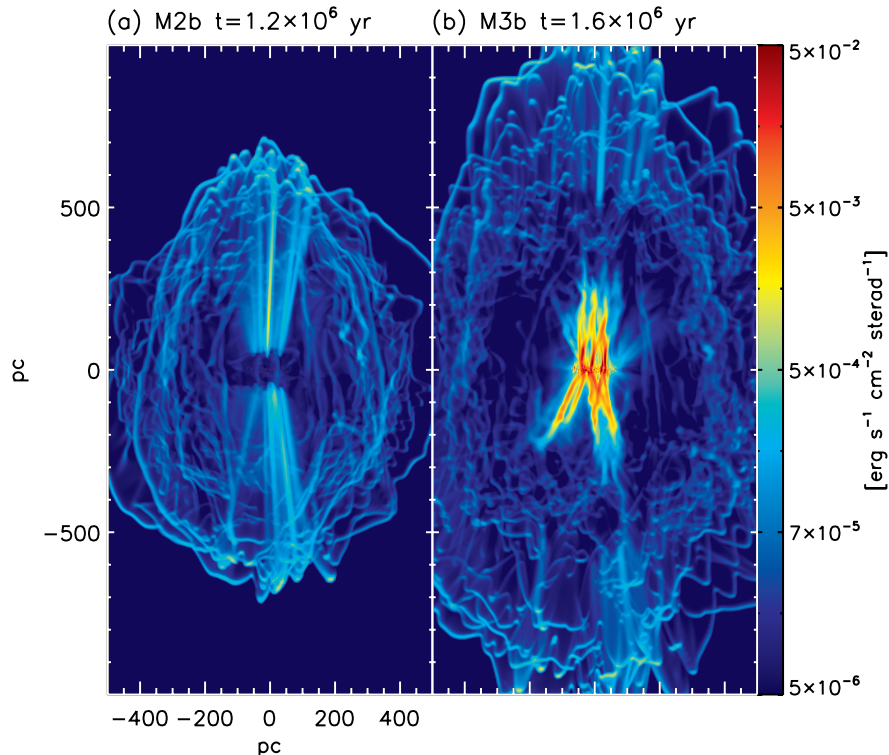


FIG. 6.— $H\alpha$ maps obtained for models M2b (left) and M3b (right). The bar on the right, gives the logarithmic gray-scale (color-scale in the online version) in $\text{erg s}^{-1} \text{cm}^{-2} \text{sterad}^{-1}$. The images were obtained by integrating the emission coefficient along lines of sight parallel to the x -axis. The distributions correspond to time-integrations of $(1.2, 1.6) \times 10^6$ yr (for models M2b and M3b, respectively).

equilibrium in the low density regime (i. e. the emission coefficient is proportional to the square of the density).

The X-ray maps corresponding to the end of the time-integrations of models M1-M4 are shown in Figure 5. These maps show that the models M1 and M4 (with low radiative losses) produce an extended, diffuse X-ray emission. On the other hand, the highly radiative models M2 and M3 produce X-ray emission concentrated to the galactic plane.

M82 shows X-ray emission which extends to large distances (few kpc) from the galactic plane (Stevens et al. 2003). Because the preferred model for this galaxy is M3 (which produces $H\alpha$ filaments which start from the galactic plane, see Figure 4 and §4.1), we see that in order to reconcile the X-ray map predicted from this model (see Figure 4) and the observed X-ray distribution of M82 we need to assume that the observed X-ray emission comes from another component. This component, e. g., could be the shock of the expanding SGW against the intergalactic medium. The emission from this shock is seen in the top and bottom parts of the frames corresponding to models M2 and M3 in Figure 5, but the shock structure is already escaping from the computational domain.

4.3. The $H\alpha$ emission at larger distances from the galaxy

Models M1-M4 extend only to 250 pc on either side of the galactic plane. As the filaments in M82 and NGC1569 extend to $\sim 0.5 \rightarrow 1$ kpc away from the plane of the galaxy, we have run models M2b and M3b (with the same parameters as M2 and M3, respectively, but with lower resolution and larger spatial extent, see §3 and Table 2) in order to explore whether or not the $H\alpha$

filaments predicted from our models do extend out to ~ 1 kpc.

In Figure 6, we show the $H\alpha$ maps predicted from models M2b (at $t = 1.2 \times 10^6$ yr) and M3b (at $t = 1.6 \times 10^6$ yr). The two times are chosen so as to show an approximate time sequence of the flow, as the two models produce similar results. It is clear that in the two models, the $H\alpha$ filaments extend to distances of $\sim \pm 500$ pc from the galactic plane. In the $H\alpha$ map of M3b, there is a transition to a more complex morphology at distances $> \pm 300$ pc from the galactic plane, which is not seen in model M2b (in which basically the same filaments are seen at larger distances).

5. CONCLUSIONS

We study the formation of filaments in the galactic winds driven by young SSCs in regions of high star formation. We study models in which the filaments are produced solely by the interaction between winds from SSCs, and do not consider the possible effects of the stratified or clumped ISM present in the galactic disk. In our models, the winds propagate into a low density, homogeneous environment, which could correspond to the intergalactic medium.

We have shown how a (\dot{M}_w/D) vs. v_w diagram can be used to determine if the interaction between the winds of SSCs are radiative, in which case cold filaments can be formed. With the (\dot{M}_w/D) vs. v_w diagram (Figure 1) one can diagnose if a galaxy with a high star formation rate will show filaments in optical emission lines, or only a galactic wind with X-ray emission. At the same time, given an observation of a galactic wind with a rich filamentary structure, one could predict the number of SSCs

which are contained within the observed galaxy.

We computed three models of dense starbursts (M1-M3) based on the observed parameters of M82, and a fourth model (M4), based on NGC253. The models are based on cluster distributions with mean separations between clusters similar to the observed values, but with spatial extents which are considerably smaller than the total extent of the starburst regions. The distributions used in the model could correspond to individual “starburst clumps” such as the ones observed in M82 by Westmoquette et al. (2007).

For the parameters of M82 we computed four models (M1-M3, and M1a) with different metallicities (from solar to 10 times solar). For the parameters of NGC253 we computed two models (M4 and M4a) with a 10 times solar metallicity. Models M1-M4 assumed a mass loss rate consistent with the average mechanical luminosity of the SSCs. Models M1a and M4a are obtained with rather extreme mass loss rates, only achievable during a short-lived phase in which the input from SN dominates over stellar winds.

For the models based on M82, we see the formation of cold, H α -emitting, filaments that extend out from the plane of the the galactic disk in the models with metallicities $\gtrsim 5 Z_{\odot}$ (models M2 and M3). We also see formation of dense filaments for the models with extreme mass loss rate at the supernova phase of the clusters (models Ma1 and M4a), where a more conservative mass loss rate did not yielded filaments (M1 and M4).

For the model based on NGC253 (M4), no filaments are produced, even for a 10 Z_{\odot} metallicity. This is consistent with the present observations of this object, in which no H α -emitting filaments have been detected. The prediction obtained from our models would be that with the distribution of SSCs of NGC253 (in pre or post SN phase), no H α filaments should exist. However, we have shown that during the SN phase (model M4a and section 3.1) the formation of cold filaments is possible in such high metallic winds. Hoopes et al. (2005) claim that the lack of evidence of filamentary structure in the galactic wind of NGC253 could simply be the result of not having deep enough H α maps of this object. In the future we will see whether or not this result is confirmed by deeper observations.

We have also computed X-ray maps in the energy range of 0.3 to 2 keV. For the highly radiative models (M2 and

M3), we find that the X-ray emission is concentrated in a region close to the galactic plane. In order to reconcile this result with the observation of extended X-ray emission in M82, we would have to assume that the emission comes from another component in the flow, which could be the shock of SGW against the intergalactic medium.

Finally, we have run two models (M2b and M3b) with the parameters based on M82 (and abundances of 5 Z_{\odot} and 10 Z_{\odot} , respectively) with lower computational resolutions but with larger spatial extents. From these runs, we find that the models produce a filamentary H α morphology that extends out to $\sim 0.5 \rightarrow 1$ kpc on each side of the galactic plane.

We end by noting that in this paper we prove that the radiative interaction between the winds from a disk-like distribution of identical SSCs (super stellar clusters) does lead to the production of dense filaments extending out to 100 \rightarrow 1000 pc away from the galactic plane. These structures produce H α emission that might correspond to the filaments observed in starburst galaxies such as M82 and NGC1569. Of course, in our models we do not consider many elements that are likely to be important in starburst galaxies. Important among these might be:

- the presence of a dense, stratified galactic disk interstellar medium,
- clumpiness in this medium,
- the existence of a distribution of sizes and ages for the SSCs,
- the effect of galactic mass loading.

There is therefore a large field for future theoretical studies on the formation of filamentary structures in starburst galaxies.

We acknowledge support from the DGAPA (UNAM) grant IN108207, from the CONACyT grants 46828-F and 61547, and from the “Macroproyecto de Tecnologías para la Universidad de la Información y la Computación” (Secretaría de Desarrollo Institucional de la UNAM). We thank Enrique Palacios, Martín Cruz and Antonio Ramírez for their support of the servers in which the simulations were carried out.

REFERENCES

- Aller, L. H. 1987, *Physics of Therma Gaseous Nebulae* (Dordrecht: Reidel), pp. 76-77
- Anders, P., de Grijs, R., Fritze-v. Alvensleben, U. & Bissantz, N., 2004, *MNRAS*, 347, 17.
- Cantó, J., Raga, A.C. & Rodríguez, L.F., 2000, *ApJ*, 536, 896.
- Chevalier, R.A. & Clegg, A.W., 1985, *Nature*, 317, 44.
- Cooper, J. L., Bicknell, Geoffrey V., Sutherland, R. S., Bland-Hawthorn, Joss, 2008, *ApJ*, 674, 157.
- Dere, K. P., Landi, E., Mason, H. E., Monsignori Fossi, B. C., & Young, P. R. 1997, *A&AS*, 125, 149.
- Griffiths, R. E., Ptak, A., Feigelson, E. D., Garmire, G., Townsley, L., Brandt, W. N., Sambruna, R. & Bregman, J. N., 2000, *Sci*, 290, 1325.
- Harris, J., Calzetti, D., Gallagher, J. S., Conselice, C. J. & Smith, D. A., 2001, *AJ*, 122, 3046.
- Hartigan, P., Raymond, J. & Hartmann, L., 1987, *ApJ*, 316, 323.
- Heckman, T. M., Armus, L., & Miley, G. K., 1990, *ApJS*, 74, 833.
- Hoopes, C. G., Heckman, T. M., Strickland, D. K.; Seibert, M., Madore, B. F., Rich, R. M., Bianchi, L., Gil de Paz, A., Burgarella, D., Thilker, D. A., Friedman, P. G., Barlow, T. A., Byun, Y., Donas, J., Forster, K., Jelinsky, P. N., Lee, Y., Malina, R. F., Martin, D. C., Milliard, B., Morrissey, P. F., Neff, S. G., Schiminovich, D., Siegmund, O. H. W., Small, T., Szalay, A. S., Welsh, B. Y. & Wyder, T. K., 2005, *ApJ*, 619, 99.
- Landi, E., Del Zanna, G., Young, P. R., Dere, K. P., Mason, H. E., & Landini, M. 2006, *ApJS*, 162, 261.
- Leitherer, C. & Heckman, T. M., 1995, *ApJ*, 96, 9.
- Lynds, C. R. & Sandage, A. R., 1963, *ApJ*, 137, 1005.
- Meynet, G., & Maeder, A. 2002, *A&A*, 390, 561.
- Melo, V.P., 2005, PhD Thesis, “Evolución e impacto de estallidos de formación de estrellas en núcleos de galaxias”, Instituto de Astrofísica de Canarias.
- Melo, V. P., Muñoz-Tuñón, C., Maíz-Apellániz, J. & Tenorio-Tagle, G., 2005, *ApJ*, 619, 270.
- O’Connell, R. W. & Mangano, J. J., 1978, *ApJ*, 221, 62.

- O'Connell, R. W., Gallagher, J. S., III, Hunter, D. A. & Colley, W. N., 1995, *ApJ*, 446, 1.
- Ohyama Y., Taniguchi, Y., Iye, M., Yoshida, M., Sekiguchi, K., Takata, T., Saito, Y., Kawabata, K. S., Kashikawa, N., Aoki, K., Sasaki, T., Kosugi, G., Okita, K.; Shimizu, Y., Inata, M., Ebizuka, N., Ozawa, T., Yadoumaru, Y., Taguchi, H. & Asai, R. 2002, *PASJ*, 54,891.
- Raga, A. C., Navarro-González, R., & Villagrán-Muniz, M. 2000, *Revista Mexicana de Astronomía y Astrofísica*, 36, 67.
- Raga, A.C., Velazquez, P.F., Cantó, J., Masciadri, E. & Rodríguez, L.F., 2001, *ApJ*, 559, L33.
- Raga, A. C., Reipurth, B. 2004, *RMxAA*, 40, 15
- Raga, A. C., de Gouveia Dal Pino, E. M., Noriega-Crespo, A., Mininni, P. D., & Velázquez, P. F., 2002, *A & A*, 392, 267.
- Raymond, J. C., Cox, D. P.& Smith, B. W., 1976, *ApJ*, 204, 290.
- Rice, W., 1993, *AJ*, 105, 67.
- Rodríguez-González, A., Cantó, J., Esquivel, A., Raga, A. C. & Velazquez, P. F., 2007, *MNRAS*, 380, 1198.
- Rockefeller, G., Fryer, C. L., Melia, F., Wang, Q. D., 2005, *ApJ*, 623, 171.
- Shoppell, P. L.& Bland-Hawthorn, J., 1998, *ApJ*, 493, 129.
- Shull, J. M., McKee, C. F. 1979, *ApJ*, 227, 131
- Stevens, I.R., Read, A. M., Bravo-Guerrero J., 2003, *MNRAS* 343, L47
- Strickland, P. K. & Stevens, I. R., 2000, *MNRAS*, 314, 511.
- Tenorio-Tagle, G., Silich, S., & Muñoz-Tuñón, C., 2003, *ApJ*, 597,279.
- Tenorio-Tagle, G., Silich, S., Rodríguez-González, A. & Muñoz-Tuñón, C., 2005, *ApJ*, 628, 13.
- Tomisaka, K. & Ikeuchi, S., 1988, *ApJ*, 330, 695.
- Westmoquette, M. S., Exter, K. M., Smith, L. J., Gallagher, J. S. 2007, *MNRAS*, 381, 894
- Westmoquette, M.S., Smith, L.J. & Gallagher III, J.S., 2008, *MNRAS*, 383, 864.